Research Article | Vol. 26, No. 23 | 12 Nov 2018 | OPTICS EXPRESS 30623
Optics EXPRESS

Multi-layer silicon nitride-on-silicon polarization-independent grating couplers

JASON C. C. MAK,[1,*] WESLEY D. SACHER,[1,2] HUANG YING,[3] XIANSHU LUO,[3,4] PATRICK GUO-QIANG LO,[3,4] AND JOYCE K. S. POON[1]

[1] *Department of Electrical and Computer Engineering, University of Toronto, 10 King's College Road, Toronto, Ontario M5S 3G4, Canada*
[2] *Kavli Nanoscience Institute, California Institute of Technology, 1200 East California Blvd, Steele Laboratory, Pasadena, CA 91125, USA*
[3] *Formerly with Institute of Microelectronics, A*STAR (Agency for Science, Technology and Research), 11 Science Park Road, Singapore Science Park II, 117685, Singapore*
[4] *Advanced Micro-Foundry Pte Ltd., 11 Science Park Road, Singapore Science Park II, 117685, Singapore*
[*] *jcc.mak@mail.utoronto.ca*

Abstract: A polarization-independent grating coupler is proposed and demonstrated in a 3-layer silicon nitride-on-silicon photonic platform. Polarization independent coupling was made possible by the supermodes and added degrees of geometric freedom unique to the 3-layer photonic platform. The grating was designed via optimization algorithms, and the simulated peak coupling efficiency was -2.1 dB with a 1 dB polarization dependent loss (PDL) bandwidth of 69 nm. The fabricated grating couplers had a peak coupling efficiency of -4.8 dB with 1 dB PDL bandwidth of over 100 nm.

1. Introduction

Grating couplers (GCs) have emerged as effective optical input/output interfaces between standard optical fibers and silicon (Si) photonic circuits [1–4]. In conventional silicon (Si) photonic platforms, GCs are formed with the single Si waveguide layer using partially or fully etched features. One dimensional (1D) Si GCs are highly polarization sensitive, which can be intuitively explained using the grating equation. For a GC to couple optical power from a waveguide mode propagating in the chip to an emission angle, θ, away from the normal of the plane of the chip, it must satisfy the phase-matching condition,

$$k_0 \bar{n}_{eff,m} = k_0 n_c sin\theta + q\frac{2\pi}{\Lambda}, \tag{1}$$

where k_0 is the free-space wavevector of the light, $\bar{n}_{eff,m}$ is the effective index of mode m in the GC, n_c is the cladding refractive index of the GC, Λ is the grating period, and q is an integer indexing the diffraction order. In a typical periodic 1D GC formed in a single waveguide layer, $\bar{n}_{eff,m}$ depends on the grating duty cycle, f. It is usually not possible to choose a duty cycle such that Eq. 1 is simultaneously satisfied for both transverse electric (TE) and transverse magnetic (TM) polarized modes, i.e., generally, $\bar{n}_{eff,TE}(f) \neq \bar{n}_{eff,TM}(f)$, leading to polarization-dependent characteristics.

Therefore, to realize a single layer polarization-independent GC (PI-GC), more degrees of freedom, beyond f, is needed such that TE and TM modes can satisfy the same condition in the right hand side in Eq. 1. This can be achieved through 2D patterns [5, 6], an intersection of 1D TE and TM gratings [7], or full freedom in the grating geometry [8]. However, thus far, such PI-GCs have exhibited limited coupling efficiency and bandwidths. Proposals require back-reflectors [5] or subwavelength features [5, 7, 8]. Defining the polarization dependent loss

#342025 https://doi.org/10.1364/OE.26.030623
Journal © 2018 Received 14 Aug 2018; revised 29 Sep 2018; accepted 9 Oct 2018; published 7 Nov 2018

Optics EXPRESS

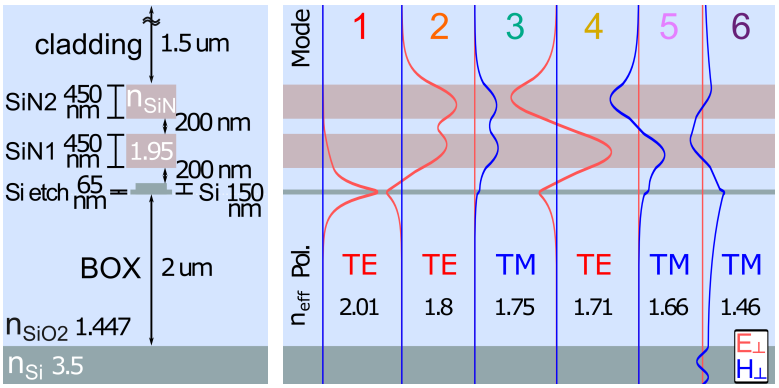

(a) (b)

Fig. 1. (a) Cross-section of the 3-layer SiN-on-Si platform in this work. Vertical dimension is to scale. Layer dimensions and refractive index at nominal center wavelength 1310 nm are indicated. (b) Profiles of the electric (red) and magnetic (blue) fields perpendicular to the plane of the modes supported by the SiN2, SiN1, and Si etch slab layers. The n_{eff} of the supermodes are annotated.

(PDL) bandwidth $\Delta\lambda_{1\text{dB PDL}}$ as the bandwidth where PDL is under 1 dB, and η_{PI} to be the maximum coupling efficiency in either polarization within the PDL bandwidth, to date, the best experimental demonstration of a PI-GC has a $\Delta\lambda_{1\text{dB PDL}}$ of 12 nm with η_{PI} of -6 dB.

Here, we present 1D PI-GCs for the O-band in the 3-layer silicon nitride (SiN)-SiN-on-silicon (Si) platform reported in [9] and [10]. The three layers supported 5 confined supermodes which allowed polarization independent coupling to be realizable using available degrees of freedom. The PI-GCs were designed by a combination of heuristics and optimization algorithms, achieving in simulation η_{PI} = -2.1 dB at 1310 nm with $\Delta\lambda_{1\text{dB PDL}}$ = 69 nm. The best fabricated device had η_{PI} = -4.8 dB at 1306 nm $\Delta\lambda_{1\text{dB PDL}}$ of >100 nm. To the best of our knowledge, this is the highest η_{PI} with largest $\Delta\lambda_{1\text{dB PDL}}$ amongst experimentally realized PI-GCs to date. This result complements the ongoing work on broadband and high peak coupling efficiency bi-layer GCs [11–15] and demonstrates the versatility of multi-layer GCs.

This work is organized as follows. In Section 2, we elaborate on the feasibility of polarization independence in the 3-layer stack, and the optimization process. Section 3 provides experimental measurements of the fabricated devices. Section 4 compares the results with a representative selection of polarization independent and polarization splitting gratings from literature, after which we summarize and conclude.

2. Design

2.1. Polarization independent coupling in a 3-layer GC

Figure 1(a) shows the waveguide layers of the 3-layer platform. To intuitively illustrate why a 1D PI-GC can potentially be designed, we examine the modes supported by slab waveguides in this platform. The purpose is to identify whether sufficient degrees of freedom exist to tailor $\bar{n}_{eff}$ for the relevant grating modes such that the modes simultaneously satisfy Eq. 1. Full numerical simulations need to be carried out for the PI-GC design to account for substrate reflections and the strong index perturbation (i.e., the guided modes alone do not fully predict the GC performance). The cross-section consisting of the thin Si etch slab and the two fully etched SiN layers, each individually single-mode for TE and TM polarizations, supports a total of 6 supermodes (modes of a system of multiple coupled optical waveguides), as illustrated in Fig. 1(b). To directly couple light from the multi-layer grating into a single layer waveguide, we consider how the

Optics EXPRESS

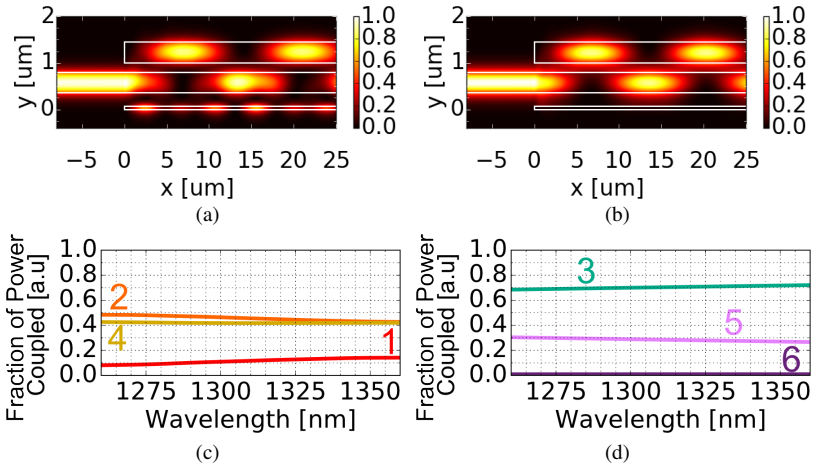

Fig. 2. (a)-(b): Power profile in the 3-layer region excited from a SiN1 slab waveguide. Outline of the waveguides are shown in white. Fundamental TE [(a)] and TM [(b)] modes of the SiN1 waveguide excite supermodes of the 3-layer region. No power resides in the Si etch layer for the TM polarization. (c)-(d): Fraction of power coupled to each supermode corresponding to fundamental TE [(c)] and TM [(d)] excitation.

supermodes are excited by an input mode from a SiN1 slab waveguide. While a TE input mode couples into the 3 TE supermodes in the 3-layer region [Fig. 2(a) and Fig. 2(c)], a TM input mode couples into only 2 TM supermodes [Fig. 2(b) and Fig. 2(d)]. This is because Mode 6 is not well confined and has very poor overlap with a TM input mode. Therefore, in total, there are 5 modes relevant for polarization independent coupling into an SiN1 slab waveguide.

The 5 relevant modes are matched by 5 degrees of freedom in the geometry of a periodic 3-layer GC that can be used to adjust $\bar{n}_{eff,m}$: 1. Fill factor in Si (f_0), 2. Fill factor in SiN1 (f_1), 3. Fill factor in SiN2 (f_2), 4. Spatial offset between the Si and SiN1 features (o_0), and 5. Spatial offset between the SiN1 and SiN2 features (o_2). These 5 degrees of freedom allow for the possibility for $\bar{n}_{eff,m}$ to be adjusted such that it is equal for all 5 confined supermodes, thus the potential for polarization insensitive operation.

2.2. *Optimization assisted design*

While satisfying the system of grating equations is a prerequisite for PI-GCs, their good performance (e.g., in terms of η_{PI} and $\Delta\lambda_{1\mathrm{dB\ PDL}}$) is not guaranteed. Therefore, in addition to these 5 degrees of freedom that adjust $\bar{n}_{eff,m}$, we include the period Λ of the grating, and the fiber position x_s and polish angle θ in the design process to maximize η_{PI} and $\Delta\lambda_{1\mathrm{dB\ PDL}}$. This results in 8 degrees of freedom for the design of a periodic 3-layer grating. We give a parameterization in Fig. 3, where we have defined the variables $w_1 = f_1\Lambda$, $g = (1 - f_1)\Lambda$, $w_0 = f_0\Lambda$, $w_2 = f_2\Lambda$ for convenience of specifying minimum feature sizes. Apodizing the grating for this parameterization will result in $2 + 6N$ variables for apodization of N teeth.

To develop a design, we used a combination of optimization algorithms and heuristics to optimize figures of merits (FOM) extracted from direct 2D Finite-Difference Time-Domain (FDTD) simulations of the design. These 2D-FDTD simulations were set up based on the parameterization in Fig. 3. The GCs are designed to couple light from an angled polished SMF-28 fiber into a SiN1 waveguide. g, w_1, w_0, w_2 are set between minimum allowable features sizes (0.4 μm for g, 0.3 μm for w_1 and w_2, and 0.18 μm for w_0) up to coarse features of around 1.3 μm corresponding to an upper limit of roughly wavelength per period, beyond which the

Optics EXPRESS

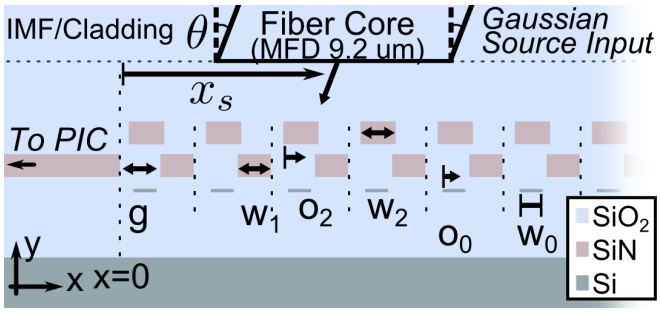

Fig. 3. Diagram of the 3-layer PI-GC simulation setup and design parameters.

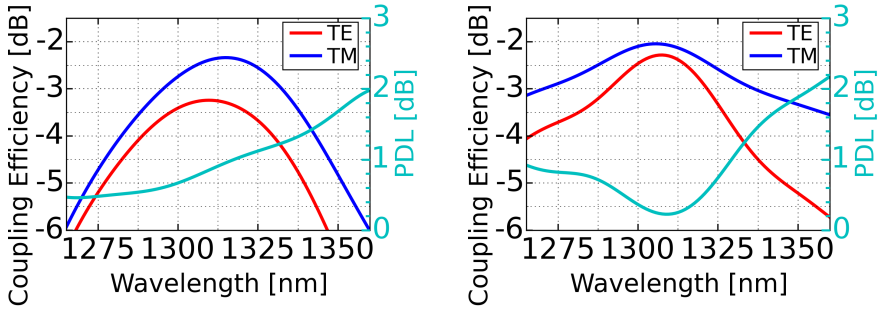

Fig. 4. Spectrum of the (a) uniform PI-GC and (b) apodized PI-GC.

resultant grating period would not be efficient for the target wavelength. The offsets o_0 and o_2 are allowed to vary approximately over an entire period, within $(-2, 0)$ μm. Due to substrate reflections and mode matching, the optimal θ cannot be known *a priori*. Therefore, the design procedure also searched over coupling angles in the range of $\theta \in (0°, 35°)$ without being limited by the total internal reflection for the cladding-air interface (43.7°). The distance between the SiN1 waveguide and the center of the fiber is x_s, which is bounded between 4 and 7 μm. A Gaussian source with mode field diameter (MFD) corresponding to SMF-28 fiber at 1310 nm injects 45° polarized light. The TE and TM transmission spectrum of the GC is taken in the SiN1 waveguide using mode overlap integrals.

We first tried to design a periodic 3-layer GC to achieve good coupling efficiency in TE and TM polarizations simultaneously. We used the average between the TE and TM coupled power at 1310 nm as the FOM for this design as it was fast to calculate using only one 2D-FDTD simulation with diagonally polarized light input into the grating. With this FOM, we ran 100 iterations of the particle swarm algorithm [16], using a population of 100 particles initialized with uniform random sampling. Since this FOM does not account for PDL and $\Delta\lambda_{1\text{dB PDL}}$, we visually inspected 20 of the top performing designs to eliminate designs with high PDL or narrow $\Delta\lambda_{1\text{dB PDL}}$ which occur when the TE and TM polarization spectra cross. From this pool of designs, we identified a design balancing good coupling efficiency and large $\Delta\lambda_{1\text{dB PDL}}$ with low PDL [see Table 1 and Fig. 4(a)]. Excluding variations of the same design from the same local optimum, the remaining designs that we had inspected had lower efficiency, higher PDL, or lower $\Delta\lambda_{1\text{dB PDL}}$.

We then apodized the periodic GC with the goal of further improving η_{PI} and decreasing the PDL, while maintaining the wide $\Delta\lambda_{1\text{dB PDL}}$ of the periodic GC design. We incrementally performed the apodization. Multiple rounds of optimization are performed, where we select

Optics EXPRESS

Table 1. Parameters for the uniform 3-layer SiN-SiN-Si polarization independent GC

g [nm]	w_1 [nm]	o_2 [nm]	w_2 [nm]	o_0 [nm]	w_0 [nm]	x_s [μm]	θ [°]
899	830	604	640	604	1047	6	33.9

Table 2. Parameters for the apodized 3-layer SiN-SiN-Si polarization independent GC

Period	g [nm]	w_1 [nm]	o_2 [nm]	w_2 [nm]	o_0 [nm]	w_0 [nm]
1	554	890	554	498	554	1246
2	887	907	523	664	600	1051
3	812	829	542	676	762	1015
4	914	874	590	670	505	1138
5	882	856	600	664	664	1103
6	784	925	482	937	678	1415
7	738	916	483	939	590	1155
8	777	930	518	594	702	1298
9	822	792	525	830	568	1484
10	919	776	338	669	587	1237
11	838	862	621	587	575	1306
12	886	1136	548	939	482	1373
13	941	799	569	680	671	1224
14	883	830	572	648	726	1047

several randomly chosen teeth at a time to be varied, with the result from the previous round as a starting point. At each round, we applied the local optimization algorithm COBYLA [17] bounded to a small region around each starting point to make gradual improvements to one of the following FOM: 1. TE coupling efficiency at 1310 nm η_{TE}, TM coupling efficiency at 1310 nm η_{TM}, the standard deviation of the PDL computed at 100 wavelengths between 1260 and 1360 nm σ_{spread} which is proportional to PDL over the O-band in linear scale, and 4. $\Delta\eta_{log} = \log_{10}[\eta_{TM}/\eta_{TE}]$ which reduces the difference in the TE and TM coupling efficiencies at the center wavelength in logarithmic scale. At each round, the FOM was selected heuristically by visual inspection based on the result of the previous round, attempting to balance the increase of the η_{PI} while minimizing the PDL. We first tried to alternate between increasing η_{TE} and η_{TM}, but this often led to an increased difference between the TE and TM spectra, or a spectral shift between the two polarizations. Applying the FOMs σ_{spread} or $\Delta\eta_{log}$ usually decreased the

Optics EXPRESS

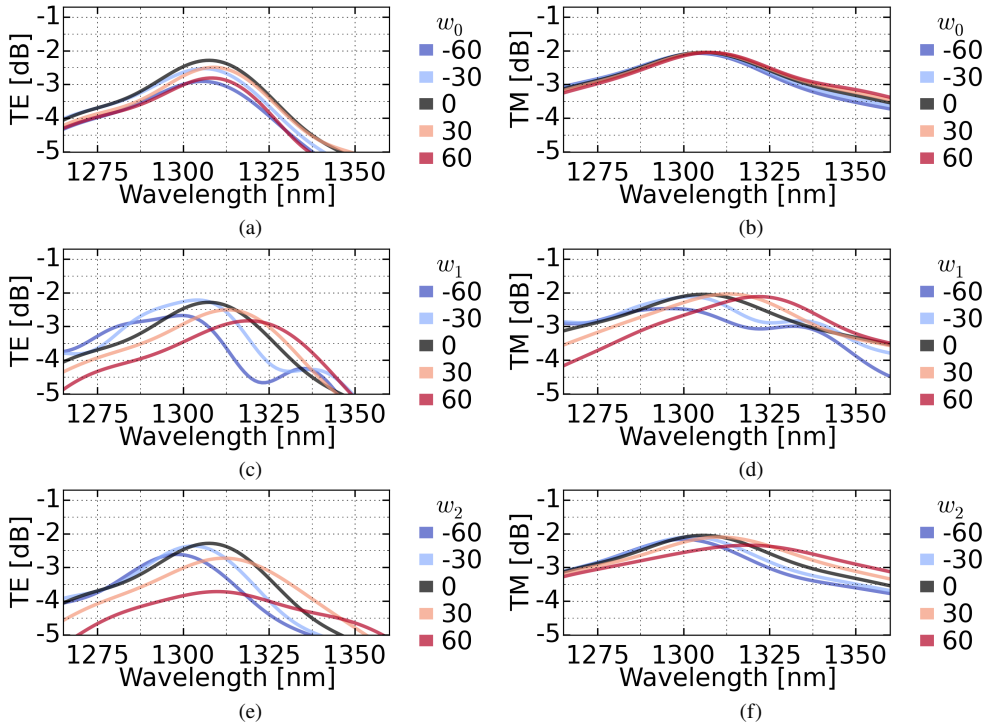

Fig. 5. Sensitivity of the apodized design to fill-factor, given as deviations from the nominal teeth widths w from Tab. 2 while the fixing the corresponding period. Variations are given in nm. (a), (c), (e): Sensitivity of the TE spectra. (b), (d), (f): Sensitivity of the TM spectra.

PDL but sometimes at a slight cost of coupling efficiency. This prompted additional attempts to increase η_{TE} and η_{TM}. Through repeated cycling of the FOM and optimization parameters, improvements became less frequent, and we chose to stop at apodized GC with spectrum shown in Fig. 4(b), with x_s = 5 μm and θ = 33.9°. Design parameter values are shown in Table 2. Both TE and TM spectra are centered at 1306 nm, with a peak coupling efficiencies of -2.3 dB and -2.1 dB, respectively. The PDL of 0.2 dB at the peak is the lowest value. PDL is below 1 dB between 1329 nm and 1260 nm. Therefore, $\Delta\lambda_{1\text{dB PDL}}$ = 69 nm and η_{PI} = -2.1 dB.

We show the impact of fabrication variation in fill-factor, interlayer spacer and interlayer offsets in Figs. 5-7 respectively. Fill-factor variations are given in Fig. 5 as deviations from the nominal teeth widths w of Tab. 2 in nm while the fixing the corresponding period. While the TM polarization spectra remains relatively robust against most ±60 nm variations, the TE polarization is prone to shifts in the center wavelength or additional losses. The most significant impact on the performance comes from variations in the SiN1 and SiN2 fill-factors, spacer thicknesses, and SiN2 offset. In these variations, the TE coupling efficiency degrade significantly. In all cases, the TE and TM spectra change in different ways with respect to the variations, which impacts PDL and $\Delta\lambda_{1\text{dB PDL}}$.

3. Experiment

The GCs were fabricated on 200mm wafers with deep UV lithography at IME A*STAR with the back-end-of-line (BEOL) platform described in [10]. The SiN layers are added on top of an active Si platform by plasma-enhanced chemical vapor deposition (PECVD), etching, and chemical mechanical polishing (CMP) steps. The GCs were 12 μm wide, and tapered down to 740 nm

Optics EXPRESS

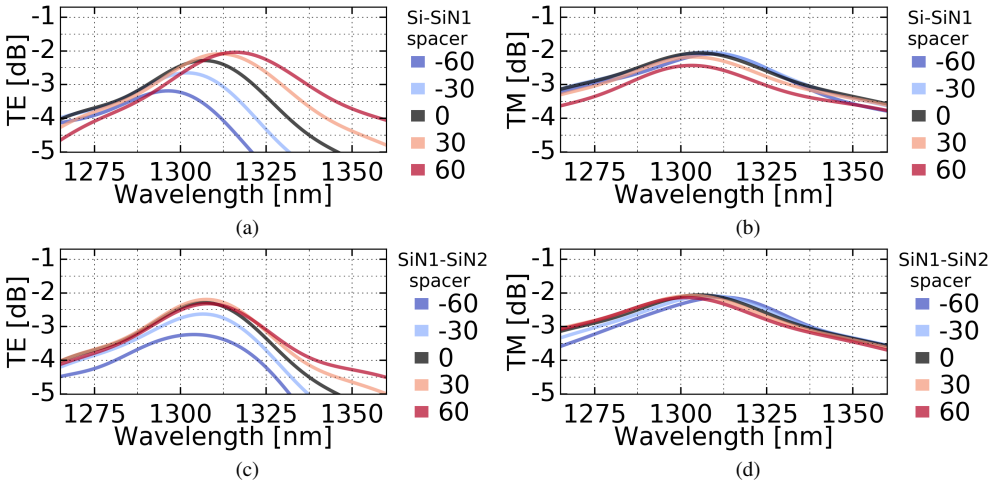

Fig. 6. Sensitivity of the apodized design to deviations from nominal interlayer spacers. Nominal spacer between Si-SiN1 and between SiN1-SiN2 are both 200 nm. Variations given in the legend are in units of nm. (a),(c): Sensitivity of the TE spectra. (b),(d): Sensitivity of the TM spectra.

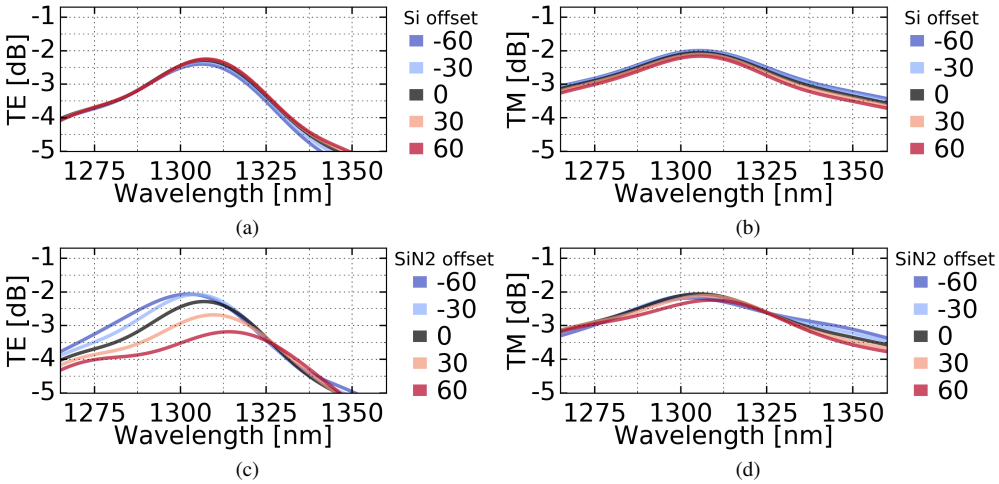

Fig. 7. Sensitivity of the apodized design to deviations from nominal interlayer offsets. Variations given in the legend are in units of nm. (a),(a): Sensitivity of the TE spectra. (d),(d): Sensitivity of the TM spectra.

waveguides by 500 μm linear tapers. The test structures consisted of pairs of GCs connected by SiN1 waveguides as shown in Fig. 8(a). The devices were measured using a fiber array polished at 34° with index fluid matching fluid (Norland IML150, refractive index $n = 1.5$) applied at the fiber-chip interface. The input laser polarization was set to TE or TM with a polarization controller (Keysight N7788B) with the polarization calibrated to Si TM GCs that were placed nearby. TM Si GCs were used as they had a higher coupling efficiency and higher PDL than TE Si GC designs at 34°. We used the large contrast between the TE and TM spectra in these TM Si GCs to determine the input polarization by minimizing/maximizing measured power at the center wavelength.

The measured spectra for TE, TM, scrambled polarization (SP) inputs, and the PDL from

Optics EXPRESS

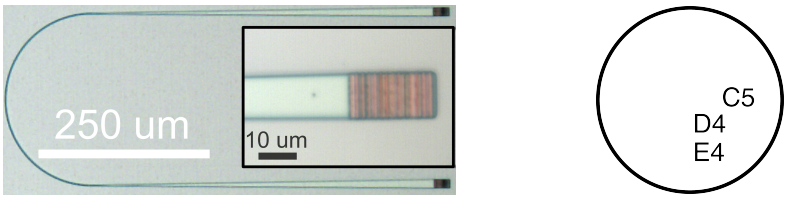

(a) (b)

Fig. 8. (a) Microscope image of fabricated GC test structure and a magnified image of a GC. (b) Wafer map of devices measured.

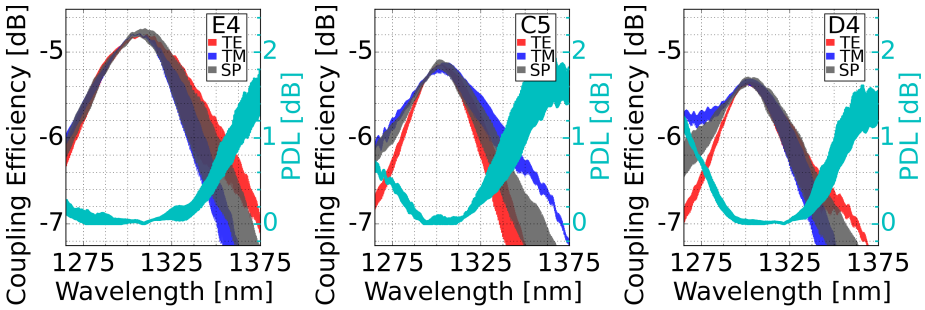

(a) (b) (c)

Fig. 9. Measured spectrum of the 3-layer PI-GCs from positions indicated in Fig. 8(b).

several devices from across the wafer with locations as indicated in Fig. 8(b) are shown in Figure 9. As determined from the free spectral range, the fringes were due to back-reflection of the GCs. From a fringe of at most -0.1 dB near the center wavelength near 1306 nm, we expect at most -22 dB back-reflection. The maximum contrast in the fringe is around -1 dB near 1340 nm, which corresponds to a back-reflection of around -12 dB. Further reduction in back-reflection can be achieved by slanting the grating teeth [18]. Device E4 achieved the best performance, with the TE and TM spectrum overlapping near 1306 nm resulting in a η_{PI} = -4.8 dB where $\Delta\lambda_{1\mathrm{dB\ PDL}}$ was ≥100 nm between <1260 nm and 1360 nm (over the entire O-band).

The measurements agreed well with simulations qualitatively, but had around -2.5 dB lower coupling efficiency. The study of geometry sensitivity of the device in Sec. 2.2 suggests while fabrication variation could partially be responsible, it is unlikely to be the predominant source of loss as we would also expect worsening of PDL and $\Delta\lambda_{1\mathrm{dB\ PDL}}$. Here, we saw that the polarization independent behavior remains well preserved. Instead, we had observed that SiN2 layer waveguides throughout the wafer experienced losses in excess of 100 dB/cm. The GC teeth uses the SiN2 layer, and an additional loss which affects TE and TM equally is consistent with a lossy SiN2 layer. The physical cause of this fabrication issue is still under investigation, but it can be avoided in future runs as this issue was not present in a separate fabrication run of this 3-layer platform reported in [9], and the subsequent fabrication of a similar passive 3-layer C-band platform [19]. Other contributions to losses include the lack of planarization of the oxide cladding, a slight mismatch in the refractive index between the index matching fluid (n = 1.5) and SiO_2, variation or uncertainty in the refractive index, slopes in the sidewalls of the grating features, variation in the layer thicknesses from planarization, and the precise position and angle polish of the optical fiber. Wafer-scale characterization of the material composition and layer thicknesses can be done in the future to ensure better fidelity with simulated results.

Optics EXPRESS

Table 3. Comparison with a representative selection of polarization independent and polarization splitting GCs.

	This Work (2018) 3-Layer PI-1D O-band		[6] (2014) SWL PI-2D C-band	[5] (2011) SWL+BR PI-2D C-band	[7] (2015) Intersection PI-1D C-band	
	Meas.	Sim.	Meas.	Sim.	Meas.	Sim.
η_{PI} [dB]	-4.8	-2.1	-6	-1.9	-7.8	-6.9
$\Delta\lambda_{PDL}$ [nm]	≥100 (1 dB)	69 (1 dB)	12 (1 dB)	≥80 (1.5 dB)	20 (0.8 dB)	≥100 (0.6 dB)
MFS [nm]	300	300	<100	140	180	<180

	[8] (2018) Shape Opt. PI-1D C-band	[20] (2016) SOI PS-2D C-band	[21] (2016) SOI PS-2D O-band	[3] (2014) SOI+BR PS-2D S-band	[22] (2013) SOI+BR PS-1D C-band
	Sim.	Meas.	Meas.	Meas.	Meas.
η_{PI} [dB]	-2.9	-5.1	-3.3	-1.95	-2.3
$\Delta\lambda_{PDL}$ [nm]	48 (1 dB)	≥40 (0.25 dB)	50 (1.2 dB)	26.5 (1 dB)	35 (1 dB)
MFS [nm]	50	220	340	≈300	171

η_{PI} is the best coupling efficiency of either polarization within the PDL bandwidth ($\Delta\lambda_{PDL}$) for the PDL given in parentheses. MFS is the minimum feature size of the device.

Abbreviations: **Meas.** Measured result, **Sim.** Simulation result, **PI** Polarization Independent, **PS** Polarization Splitting, **SWL** Subwavelength, **Shape Opt.** Shape Optimization, **SOI** Silicon on Insulator, **BR** Back-reflector.

4. Discussion

Table 3 compares this present work with a representative selection of PI-GCs and polarization splitting (PS) GCs from literature. This work is the first demonstration of GCs that uses supermodes in a multi-layer platform to effect polarization insensitive operation. Compared to other PI-GCs in a single waveguide layer, our approach does not require post-processing to add a back-reflector to achieve high coupling efficiency (such as comparing between simulation results in [5]), and uses coarser features more amenable to foundry fabrication. To the best of our knowledge, our design is the current best experimental demonstration of a PI grating with respect to PDL bandwidth and insertion losses.

The simulated coupling efficiency and bandwidth of our PI-GC is competitive with PS-GCs. PS-GCs are amenable for polarization diversity and are suited to single layer Si photonic platforms. However, with the introduction of SiN waveguide layers on Si, it is possible to realize components in the SiN layer that exhibit much reduced birefringence such that polarization diversity may not be needed for coarse wavelength division multiplexing (e.g., see [23] for a SiN polarization

Optics EXPRESS

insensitive wavelength demultiplexer), halving the required footprint.

Although optimization methods have been used to automate the generation of designs, the selection of the designs was largely owed to heuristic evaluations of the device performance. The optimizations used simple FOMs (i.e., single objective each time) and thus required human intervention to guide the procedure toward a final design. Because of the cycling of different FOMs, it is difficult to evaluate the optimality of the solution, although the gradual stalling of improvements suggest the design may be at a local optima of some of the FOMs. Other better performing designs may be possible. For future work, we can adopt a more systematic approach that uses multi-objective optimization or re-define a combined FOM of all the relevant metrics (e.g., η_{PI}, PDL, $\Delta\lambda_{1\mathrm{dB\ PDL}}$) that is used throughout the optimization. More systematic methods will provide better insight into design trade-offs and optimality in future designs.

5. Conclusion

In summary, we have proposed and demonstrated PI-GCs in a 3-layer SiN-on-Si platform. The polarization insensitivity was made possible by the supermodes and degrees of geometric freedom in the platform. A design was found by successively applying optimizations, each of which targeted a different FOM to optimize for a particular spectral feature. The PI GC achieved η_{PI} = -4.8 dB at 1306 nm with $\Delta\lambda_{1\mathrm{dB\ PDL}}$ of $\geq$100 nm, the first demonstration of a 3-layer GC and, to the best of our knowledge, the highest measured performance for PI-GCs to date. The work shows the versatility of multi-layer integrated photonic platforms. The results also suggest extensions of multi-layer GCs to spatial division multiplexing, by similarly coupling different input spatial modes to selected layer supermodes. Optimization based design methodologies are particularly necessary to navigate the large number of degrees of freedom in multi-layer photonics.

Funding

Natural Sciences and Engineering Research Council (NSERC); Huawei Technologies Canada.

References

1. F. Van Laere, T. Claes, J. Schrauwen, S. Scheerlinck, W. Bogaerts, D. Taillaert, L. O'Faolain, D. Van Thourhout, and R. Baets, "Compact focusing grating couplers for silicon-on-insulator integrated circuits," IEEE Photon. Technol. Lett. **19**, 1919–1921 (2007).
2. W. S. Zaoui, A. Kunze, W. Vogel, M. Berroth, J. Butschke, F. Letzkus, and J. Burghartz, "Bridging the gap between optical fibers and silicon photonic integrated circuits," Opt. Express **22**, 1277–1286 (2014).
3. L. B. Verslegers, A. Mekis, T. Pinguet, Y. Chi, G. Masini, P. Sun, A. Ayazi, K. Y. Hon, S. Sahni, S. Gloeckner, C. Baudot, F. Boeuf, and P. D. Dobbelaere, "Design of low-loss polarization splitting grating couplers," in "Advanced Photonics for Communications," (Optical Society of America, 2014), p. JT4A.2.
4. J. S. Lee, L. Carroll, C. Scarcella, N. Pavarelli, S. Menezo, S. Bernabé, E. Temporiti, and P. O'Brien, "Meeting the electrical, optical, and thermal design challenges of photonic-packaging," IEEE J. Sel. Top. Quantum Electron. **22**, 409–417 (2016).
5. X. Chen and H. K. Tsang, "Polarization-independent grating couplers for silicon-on-insulator nanophotonic waveguides," Opt. Lett. **36**, 796–798 (2011).
6. Z. Cheng and H. K. Tsang, "Experimental demonstration of polarization-insensitive air-cladding grating couplers for silicon-on-insulator waveguides," Opt. Lett. **39**, 2206–2209 (2014).
7. J. H. Song, F. E. Doany, A. K. Medhin, N. Dupuis, B. G. Lee, and F. R. Libsch, "Polarization-independent nonuniform grating couplers on silicon-on-insulator," Opt. Lett. **40**, 3941–3944 (2015).
8. L. Su, R. Trivedi, N. V. Sapra, A. Y. Piggott, D. Vercruysse, and J. Vučković, "Fully-automated optimization of grating couplers," Opt. Express **26**, 4023–4034 (2018).
9. W. D. Sacher, Z. Yong, J. C. Mikkelsen, A. Bois, Y. Yang, J. C. C. Mak, P. Dumais, D. Goodwill, C. Ma, J. Jeong, E. Bernier, and J. K. S. Poon, "Multilayer silicon nitride-on-silicon integrated photonic platform for 3D photonic circuits," in "Conference on Lasers and Electro-Optics," (Optical Society of America, 2016), p. JTh4C.3.
10. W. D. Sacher, J. C. Mikkelsen, Y. Huang, J. C. C. Mak, Z. Yong, X. Luo, Y. Li, P. Dumais, J. Jiang, D. Goodwill, E. Bernier, P. G. Lo, and J. K. S. Poon, "Monolithically integrated multilayer Silicon Nitride-on-Silicon waveguide platforms for 3-D photonic circuits and devices," Proc. IEEE pp. 1–14 (2018).
11. W. D. Sacher, Y. Huang, L. Ding, B. J. F. Taylor, H. Jayatilleka, G.-Q. Lo, and J. K. S. Poon, "Wide bandwidth and high coupling efficiency Si3N4-on-SOI dual-level grating coupler," Opt. Express **22**, 10938–10947 (2014).

Optics EXPRESS

12. W. D. Sacher, Y. Huang, G.-Q. Lo, and J. K. S. Poon, "Multilayer silicon nitride-on-silicon integrated photonic platforms and devices," J. Lightw. Technol. **33**, 901–910 (2015).
13. J. C. C. Mak, Q. Wilmart, S. Olivier, S. Menezo, and J. K. S. Poon, "Silicon nitride-on-silicon bi-layer grating couplers designed by a global optimization method," Opt. Express **26**, 13656–13665 (2018).
14. M. T. Wade, F. Pavanello, R. Kumar, C. M. Gentry, A. Atabaki, R. Ram, V. Stojanović, and M. A. Popović, "75% efficient wide bandwidth grating couplers in a 45 nm microelectronics CMOS process," in "Optical Interconnects Conference (OI), 2015 IEEE," (IEEE, 2015), pp. 46–47.
15. A. Michaels and E. Yablonovitch, "Inverse design of near unity efficiency perfectly vertical grating couplers," Opt. Express **26**, 4766–4779 (2018).
16. Y. Shi and R. C. Eberhart, "Parameter selection in particle swarm optimization," in "International Conference on Evolutionary Programming," (Springer, 1998), pp. 591–600.
17. M. J. D. Powell, "A direct search optimization method that models the objective and constraint functions by linear interpolation," in "Advances in optimization and numerical analysis," (Springer, 1994), pp. 51–67.
18. D. Vermeulen, Y. De Koninck, Y. Li, E. Lambert, W. Bogaerts, R. Baets, and G. Roelkens, "Reflectionless grating couplers for Silicon-on-Insulator photonic integrated circuits," Opt. Express **20**, 22278–22283 (2012).
19. W. D. Sacher, J. C. Mikkelsen, P. Dumais, J. Jiang, D. Goodwill, X. Luo, Y. Huang, Y. Yang, A. Bois, P. G.-Q. Lo, E. Bernier, and J. K. S. Poon, "Tri-layer silicon nitride-on-silicon photonic platform for ultra-low-loss crossings and interlayer transitions," Opt. Express **25**, 30862–30875 (2017).
20. J. Zou, Y. Yu, and X. Zhang, "Two-dimensional grating coupler with a low polarization dependent loss of 0.25 dB covering the C-band," Opt. Lett. **41**, 4206–4209 (2016).
21. W. Wu, T. Lin, T. Chu, and H. Zhang, "CMOS-Compatible High Efficiency Polarization Splitting Grating Coupler near 1310nm," in "Asia Communications and Photonics Conference," (Optical Society of America, 2016), pp. AS2F–4.
22. W. S. Zaoui, A. Kunze, W. Vogel, and M. Berroth, "CMOS-compatible polarization splitting grating couplers with a backside metal mirror," IEEE Photon. Technol. Lett. **25**, 1395–1397 (2013).
23. J. C. Mikkelsen, A. Bois, T. Lordello, D. Mahgerefteh, and J. K. S. Poon, "Polarization-insensitive silicon nitride Mach-Zehnder lattice wavelength demultiplexers for CWDM in the O-band," Under preparation (2018).